

SAMPLE CALCULATIONS
FOR
AIR FLOW IN A GLOVEBOX ROOM

C.W. Hirt and R.P. Harper
Flow Science, Inc.
March 1988

PURPOSE

A preliminary set of calculations has been undertaken to demonstrate the utility of the FLOW-3D computer program for investigating air flow patterns in glovebox rooms. Of particular interest are comparisons between different arrangements of outlet vents.

Because these calculations are only meant to be demonstrations, they have been restricted to two-dimensional slices through a typical room arrangement. It is emphasized that the real problem involves important three-dimensional flow effects that should be considered in any actual study.

To make these calculations interesting we have assumed a rather strong exhaust flow through the face of one glovebox. We have also investigated the influence on the computed results of including a two-equation turbulence model.

THE MODEL

Our typical room cross section is 11 ft wide and 10 ft high. There are rows of gloveboxes along each side of the room; the boxes extend into the room 31 inches from the side walls, have bases 42 inches above the floor, and are 39 inches high. The top corners of the boxes are sloped 30 degrees from the vertical, as shown in Fig. 1A. In this plot asterisks mark cells in the computing mesh that are completely blocked by obstacles. The corresponding mesh is shown in Fig. 1B. The mesh consists of 12 zones across the room and 16 in the vertical direction (with one additional zone to represent the bottom boundary condition). The total number of zones defining the interior of the room is $12 \times 16 = 192$. Nonuniform cell spacing has been used to increase the resolution near the face of the left box in order to better define an exhaust flow into the box. Grid lines have also been set to coincide with the straight sides of the boxes.

The structure at the bottom of the plot, Fig. 1A, represents the floor with a vent hole in the center of width 2 ft. A constant pressure was maintained in this hole region as a boundary condition. We could have specified an outflow velocity instead of using a fixed pressure, but then it would have been necessary to carefully set the total in and out flow rates over the entire computational region to be exactly zero (because of an incompressible flow assumption). The constant pressure assumption allows the flow to automatically adjust and should not significantly influence the final flow pattern.

A uniform inflow was specified across the entire top of the room at 0.214 ft/s, which corresponds to a flow volume equal to seven times the room volume per hour. At the face of the glovebox on the left side we assumed a flow through a 7 inch opening at the bottom of its vertical face. The flow velocity was taken to be 2.08 ft/s, which is an order of magnitude larger than the ventilation inlet flow velocity. Actually, in the model we did not explicitly set this velocity, but instead, defined a mass sink to exist at the face of the glovebox. This technique was used because it did not require any changes to the FLOW-3D program, while the addition of an outflow velocity at this location would have necessitated a change to the boundary condition subroutine. In any case, both techniques are equivalent in our simulation since we are considering purely incompressible flow without heat conduction.

Only steady-state flow results are of interest in this application. To accelerate the convergence to steady state we used a large pressure iteration convergence criterion (with no over-relaxation) which limited iterations to one per cycle. This means the transient approach to steady conditions is not physically meaningful. Steadiness was measured by monitoring the mean kinetic energy in the computational region. When the mean kinetic energy settled down to a constant value, it was assumed that a steady condition had been reached. For example, Fig. 2 shows the mean kinetic energy history for the first case to be described in the next section.

COMPUTATIONAL RESULTS

Our results are presented in the form of plots of computed velocities, pressures, and in the case of turbulence, the turbulent viscosity. Since these plots are generated by the code's postprocessor, it is possible to make plots of other quantities or enlarged plots of selected regions of the flow. In fact, we used this postprocessing capability in the first example to

enlarge the flow regions underneath the gloveboxes. Because of the low velocities in these regions, they did not show up clearly in the full room plot. In later examples these subregion plots were requested in the problem definition so they did not have to be separately generated. The ability to do postprocessing is an important feature of FLOW-3D, particularly in three-dimensional situations where it is rarely possible to guess beforehand where all the interesting flow features will be.

Case 1: Center Floor Vent

In glovebox rooms the outlet vents for the ventilation system typically consist of four or six vents distributed on or near the floor. This feature is one reason the flow problem is truly three dimensional. To have a reasonable two-dimensional approximation we must decide on how to redistribute these vents into an equivalent two-dimensional vent. Let's assume there are 4 vents of size 2 by 3 ft distributed along the center of the floor with the 3 ft dimension aligned with the long length of the room. Let us also assume the room is 44 ft long (four times its width). In taking a cross section we are likely to intersect a vent with probability $12/44$. If our cross section intersects a vent, the full vent outflow would be seen, while at a cross section not intersecting a vent there would be no outflow. This suggests reducing the actual outflow velocity to a value $12/44$ times smaller to represent the outflow in an average cross section. Using this reduced velocity in a two-dimensional vent that runs down the entire length of the room we find that the necessary vent width, to have the correct total volume rate of flow, is 2 ft. This is the basis for all our calculations.

The computed, steady state velocity distribution is given in Fig. 3. The incoming flow sweeps nicely across the faces of the gloveboxes before exiting through the floor vent. A definite asymmetry is apparent in the flow because of the secondary exhaust through the face of the glovebox on the left. Under the right-hand box there is a weak recirculation region. This is shown more clearly in Fig. 6, which contains an enlargement of that region. A similar plot of the flow under the left glovebox, Fig. 5, indicates a mostly stagnant region.

A plot of the steady-state pressure distribution is shown in Fig. 4. These pressures are relative to a zero reference value at the floor outlet and are in peculiar units since we normalized the air density to unity. To convert to pounds per square inch one must multiply the calculated values by $1.123E-6$, which makes the maximum pressure variation calculated in the room very small.

Case 2: Floor Vent with Turbulence

Having a stagnation region under the left-hand box does not seem completely realistic and is probably a result of ignoring viscous effects. (There is some numerical smoothing because of the crudeness of the mesh, but this so-called "numerical viscosity" does not act quite like a real viscosity.) Including a molecular viscosity would not noticeably change the flow because the Reynolds number for this case is quite large (of order 40,000). On the other hand the Reynolds number is large enough to suggest that there will be some turbulence.

FLOW-3D has several turbulence capabilities of which the most advanced is a two-equation transport model (i.e., $k-\epsilon$ model). To see how the flow might change with turbulence the calculation was repeated using this model. As an inflow boundary condition for the turbulence we assumed a low intensity equal to 1% of the incoming flow kinetic energy and a characteristic length scale of 3.0 inches.

Figure 7 shows the resulting velocity field. In this case the flow is different under the boxes as can be seen from Figs. 9-10. Now under the left box, Fig. 9, we see a counterclockwise flowing vortex. This flow structure is driven by the flow entering the face of the glovebox through turbulent momentum transfer. In fact, the maximum level of turbulent viscosity is near the face of the left glovebox, Fig. 8. The maximum viscosity value computed is about three orders of magnitude larger than the molecular viscosity of air.

Case 3: Side Vents with Turbulence

In this last example we move the floor exhaust to the side walls under the gloveboxes. The two foot wide floor vent has been split into two one-foot high side vents. Here again we have elected to use specified pressure boundaries at these outlets, and the exhaust through the left glove box face has been kept at the same flow rate as in the previous cases.

Velocities computed for this case are shown in Fig. 11, viscosity contours are given in Fig. 12, and localized flows under the gloveboxes are shown in Figs. 13-14. (The corners of the gloveboxes where they meet the side walls have been incorrectly plotted with mesh cell diagonals because of a minor input error in defining the walls. This plotting error does not influence the computed results.) The computed flow is again seen to sweep nicely across the faces of the gloveboxes, indicating that this configuration is not likely to expose workers to accidental releases of pollutants.

The side vent case is also superior to the central floor vent in that it eliminates, or at least reduces, the recirculating regions under the boxes (see Figs. 13-14). Since contaminants could be trapped in recirculating regions, the side vent model should be more efficient in cleansing the room of contaminants.

CONCLUSIONS

We must again stress that these calculational examples are only meant as demonstrations and should not be used as a basis for deciding on a proper venting system for any real situation. It is essential that three-dimensional effects be included in any actual investigation of venting characteristics.

What these examples have shown, however, is that the FLOW-3D program has considerable potential for aiding in the design of efficient and safe ventilation systems. Even simple, qualitative observations, such as the differences in recirculation region sizes and locations, can offer useful insight into the probable efficiency of one design versus another.

A real advantage of FLOW-3D is the flexibility it offers in modeling a wide variety of phenomena with relatively little effort on the part of a user. For example, the entire input to the code for Case 3 is given in Fig. 15 in the form of a Namelist input file. This file contains all the mesh, obstacle, boundary condition, and physical data needed to set up and run the problem. It also contains specific graphic output requests and all necessary computational parameters.

FLOW-3D could be used additionally to model thermal convection in the room with or without internal heat sources, or used to track marker particles (i.e., passive contaminants), or it could even track the release of a heavy gas using a two-fluid option.

OBSTACLE PLOT (X-Z PLANE AT J= 2)

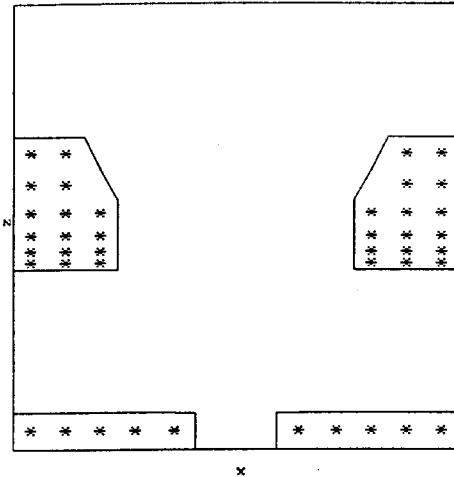


Fig. 1A.

Obstacle configurations with the bottom obstacle defining a fixed pressure outlet vent.

X-Z MESH

	X	Z
NUMBER OF CELLS-	32	17
SMALLEST CELL-	0.6107E-03	2.9202E-03
LARGEST CELL-	2.082E-03	0.747E-03
MAXIMUM CELL RATIO-	3.282E+00	2.642E+00
	AT CELL 9	AT CELL 30

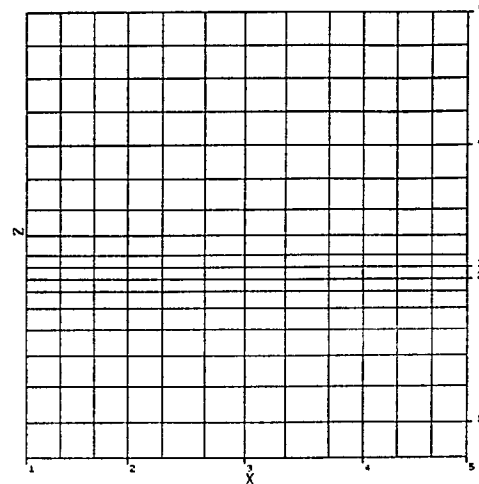


Fig. 1B.

Mesh used for all calculations.

ESTIMATED MEAN KINETIC ENERGY

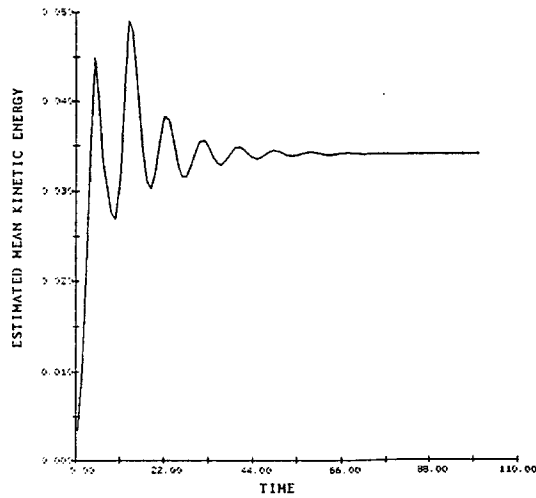


Fig. 2.

Time history of mean kinetic energy in the mesh illustrating convergence to a steady state.

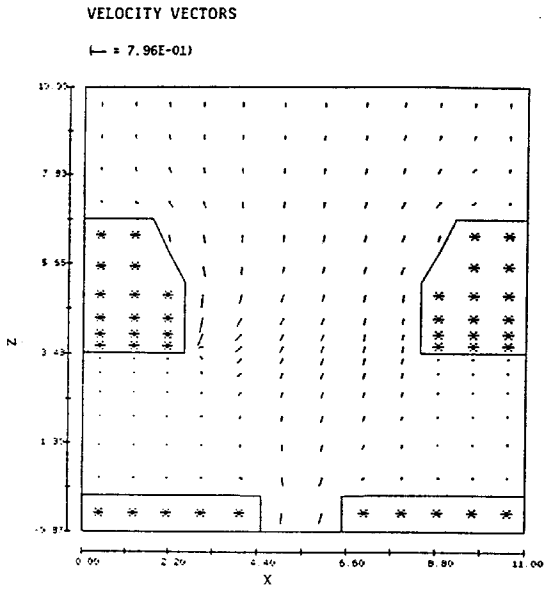


Fig. 3.
Velocity field with floor vent and no turbulence.

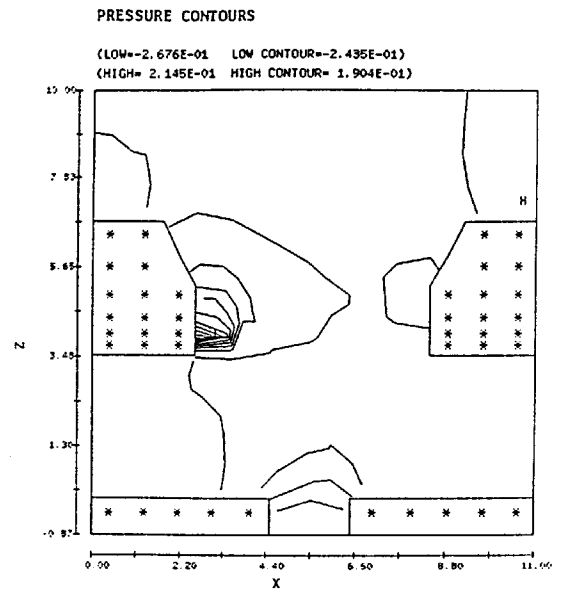


Fig. 4.
Pressure contours with floor vent and no turbulence.

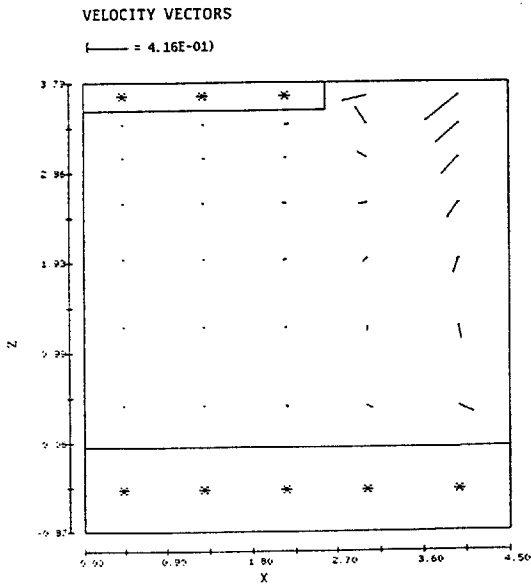


Fig. 5.
Flow under left glovebox showing stagnation region.

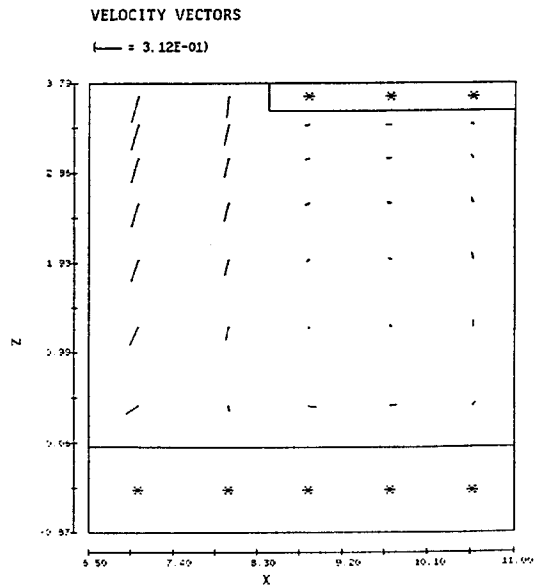


Fig. 6.
Flow under right glovebox showing counterclockwise eddy.

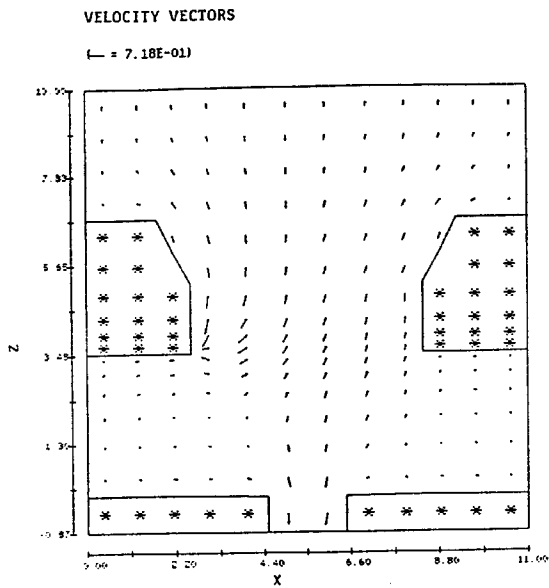


Fig. 7
 Velocity field with floor vent and turbulence effects.

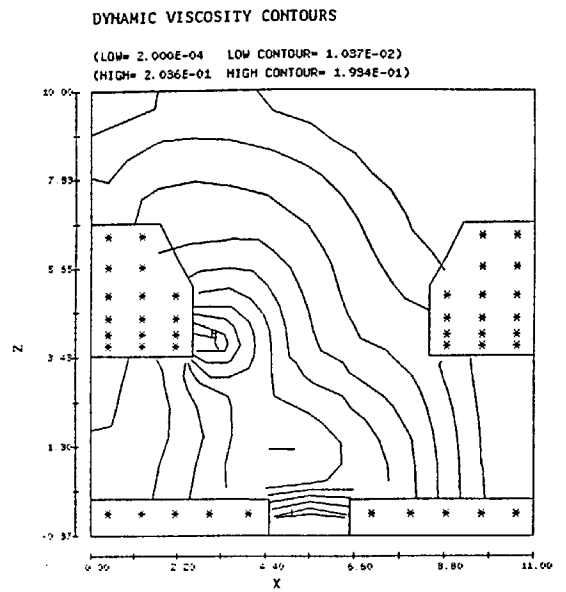


Fig. 8.
 Turbulent viscosity contours with floor vent.

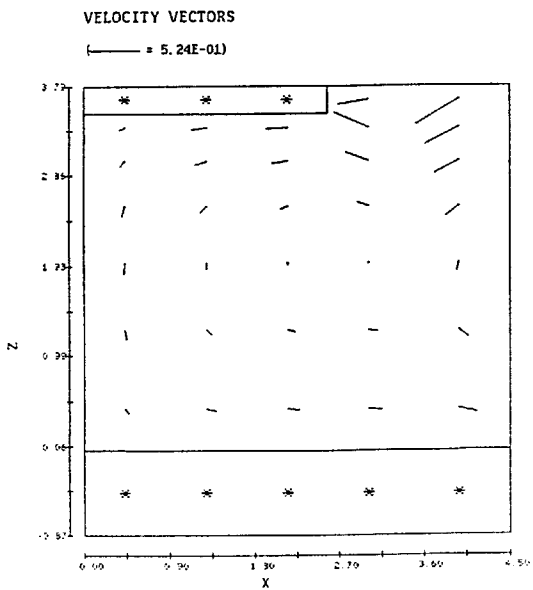


Fig. 9.
 Flow under left glovebox with turbulence showing counter-clockwise eddy. Compare with Fig. 5.

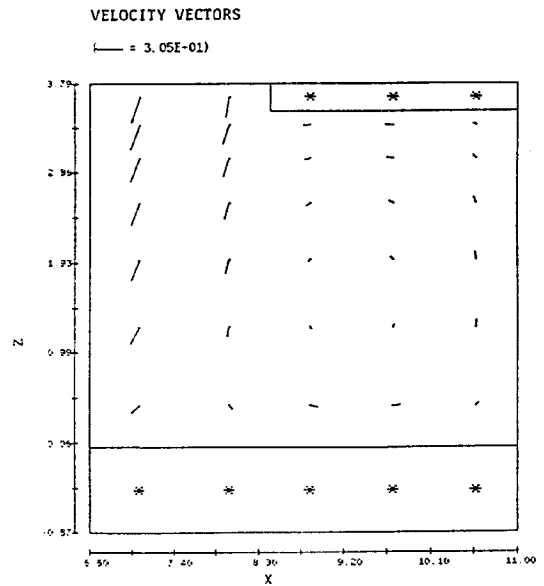


Fig. 10.
 Flow under right glovebox with turbulence showing a counter-clockwise eddy. Compare with Fig. 6.

VELOCITY VECTORS

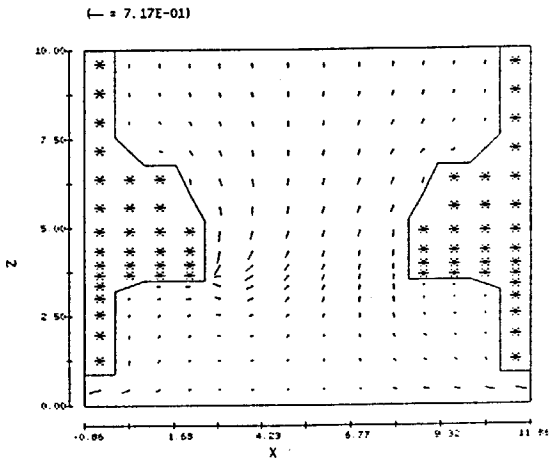


Fig. 11.
Velocity field with side vents and turbulence.

DYNAMIC VISCOSITY CONTOURS

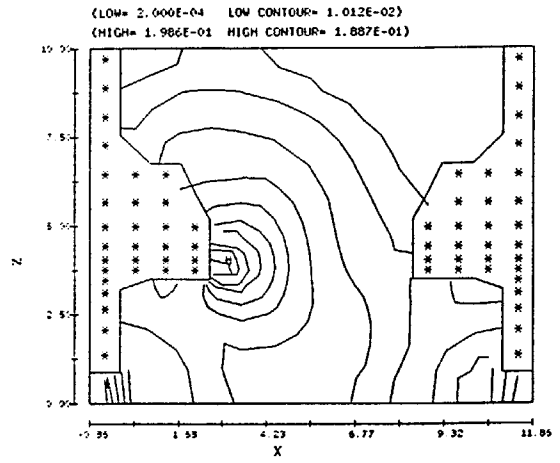


Fig. 12.
Turbulent viscosity contours for side vent case.

VELOCITY VECTORS

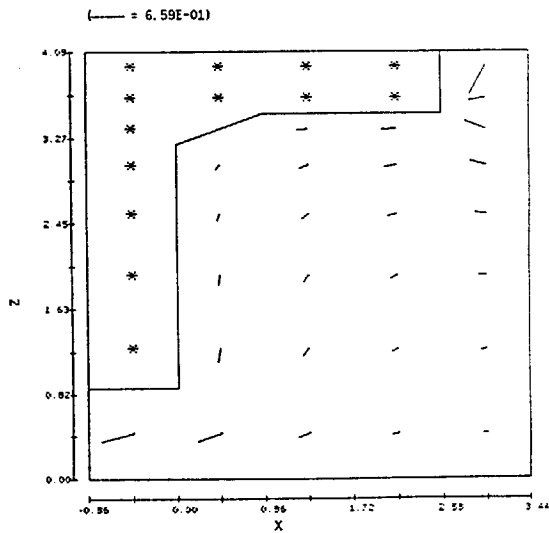


Fig. 13.
Flow under left glovebox with side vent.

VELOCITY VECTORS

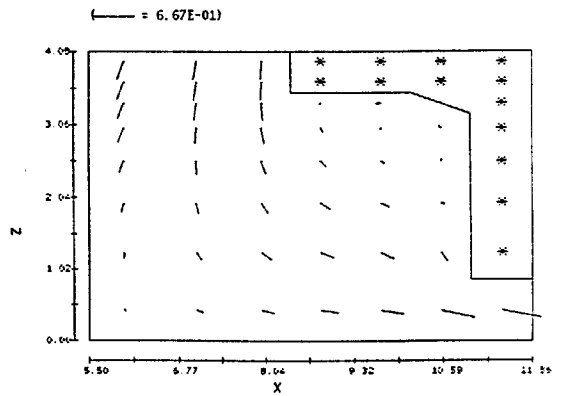


Fig. 14.
Flow under right glovebox with side vent.

GLOVEBOX VENT 3

```

$XPUT
  IFVIS=3,          TKEBCT(1,6)=2.0E-4,  TLEN=0.25,
  MUI=2.0E-4,      WL=5,                WR=5,
  CON=0.45,        TWFIN=100.,          DELT=0.5,
  PRDPT=1000.,    PLTDT=10.,
  WT=6,           WBCT(1,6)=-0.214,    OMEGA=1.0,
  EPSI=1.E+6,     IQSR=1,              AVRCK=-2.5,
$END
$MESH
  PX(2)=2.583,     PX(3)=5.5,                PX(4)=8.417,
  PX(5)=11.0,     SIZEX(3)=1.0,          NXCELT=11,
  PY(2)=1.0,      NYCELT=1,
  PZ(2)=3.5,      PZ(3)=3.792,          PZ(4)=6.75,
  PZ(5)=10.0,    SIZEZ(3)=0.292,       NZCELT=15,
  NZCELL(1)=6,   NZCELL(3)=5,
$END
$OBS
  NOBS=3,
  IOFO(1,1)=1,    CZ(1)=1.0,              CC(1)=-6.75,
  ZL(1)=3.5,
  IOFO(2,1)=2,    IOH(2)=0,              CZ(2)=1.0,
  CC(2)=-6.75,    XL(2)=2.584,          XH(2)=8.416,
  IOFO(3,1)=3,    CZ(3)=-1.0,           CX(3)=2.0,
  CC(3)=-11.751,  XL(3)=8.4,            IOH(3)=0,
  IOFO(4,1)=4,    CZ(4)=-1.0,           CX(4)=-2.0,
  CC(4)=10.249,   IOH(4)=0,             XH(4)=2.6,
  IOFO(1,2)=5,    CX(5)=1.0,            CC(5)=-2.584,
  ZL(5)=3.505,    ZH(5)=4.08,          QSROBS(1,2)=-1.213,
  IOFO(1,3)=6,
  CC(6)=-1.0,     XH(6)=0.01,           ZL(6)=0.8747,
  IOFO(2,3)=7,
  CC(7)=-1.0,     XL(7)=10.99,         ZL(7)=0.8747,
$END
$FL
$END
$BF
$END
$TEMP
$END
$GRAFIC
  NVPLTS=3,       NCPLTS=2,              KONTYP(2)=9,
  IV2(1)=6,       KV2(1)=9,
  IV1(2)=9,       KV2(2)=9,
$END
$PARTS
$END

```

Fig. 15. Input file for Case 3 with side vents.